

# MedVisionLlama: Leveraging Pre-Trained Large Language Model Layers to Enhance Medical Image Segmentation

Gurucharan Marthi Krishna Kumar  
Montreal Neurological Institute, McGill University  
gurucharan.marthikrishnakumar@mail.mcgill.ca

Aman Chadha  
Amazon  
aman@amanchadha.com

Janine Mendola  
Dept. of Ophthalmology, McGill University  
janine.mendola@mcgill.ca

Amir Shmuel  
Montreal Neurological Institute, McGill University  
amir.shmuel@mcgill.ca

## Abstract

*Large Language Models (LLMs), known for their versatility in textual data, are increasingly being explored for their potential to enhance medical image segmentation, a crucial task for accurate diagnostic imaging. This study explores enhancing Vision Transformers (ViTs) for medical image segmentation by integrating pre-trained LLM transformer blocks. Our approach, which incorporates a frozen LLM transformer block into the encoder of a ViT-based model, leads to substantial improvements in segmentation performance across various medical imaging modalities. We propose a Hybrid Attention Mechanism that combines global and local feature learning with a Multi-Scale Fusion Block for aggregating features across different scales. The enhanced model shows significant performance gains, including an average Dice score increase from 0.74 to 0.79 and improvements in accuracy, precision, and the Jaccard Index. These results demonstrate the effectiveness of LLM-based transformers in refining medical image segmentation, highlighting their potential to significantly boost model accuracy and robustness. The source code and our implementation are available at: <https://bit.ly/3zf2CVs>*

potential in improving the accuracy of medical image analysis [4, 15].

Despite their promise, ViTs in biomedical imaging face substantial challenges. Training these models requires extensive, meticulously labeled datasets, and creating such datasets in biomedical imaging is particularly burdensome due to the necessity of expert knowledge [25]. Optimizing ViTs is challenging due to the need for extensive parameter tuning, which requires deep architectural knowledge and significant computational resources, often surpassing practical limits in terms of time and cost.

This research explores methods to improve performance of ViTs in biomedical imaging while avoiding the need for larger datasets or excessive computational resources. LLMs trained on extensive textual data demonstrate notable versatility, even extending to computer vision [1, 22]. They can interpret visual tokens and integrate them into structured formats within multimodal frameworks, using linear projections or cross-attention mechanisms to process these tokens.

Our approach draws inspiration from previous studies involving the use of pre-trained LLMs for visual token processing [25, 30]. Our method involves using a pre-trained LLM transformer block as a visual encoder layer, significantly deviating from traditional Vision-Language Model (VLM) designs [26, 49]. This method operates independently of language prompts, inputs, or outputs, allows for training from scratch without needing pre-trained backbones like CLIP [31], and simplifies the use of LLMs by decoupling them into separate transformer blocks.

This method proves particularly advantageous for medical image segmentation tasks, enabling a wide range of applications. By employing a simple yet under-explored approach, we find that integrating a frozen transformer block from pre-trained LLMs as a visual encoder layer improves performance. Additionally, our examination of various LLMs and transformer blocks reveals that the effectiveness

## 1. Introduction

Medical imaging, including MRI, X-rays, and microscopy, is vital in healthcare by providing critical visual data for diagnosing diseases and formulating treatment plans. However, interpreting these images is a challenging task requiring significant expertise. Issues like low resolution and noise in scanned images can lead to misdiagnosis, resulting in incorrect or delayed treatments that negatively impact patient health [33]. Recent advancements in deep learning, particularly with Convolutional Neural Networks (CNNs) and Vision Transformers (ViTs) [11], have shown

of frozen LLM transformers in visual encoding is a consistent phenomenon, offering significant potential for enhancing medical image analysis. In summary, our paper presents the following key contributions.

- We introduce a frozen transformer block from a pre-trained LLM network into the encoder of a ViT-based medical image segmentation model, significantly improving both performance and accuracy.
- We propose an innovative Hybrid Attention Mechanism that combines efficient and channel attention to balance global and local feature learning, along with a Multi-Scale Fusion Block that aggregates features across various scales to enhance segmentation precision.
- We evaluate the effect of incorporating a frozen LLM transformer block on segmentation performance across 10 different medical imaging modalities, supported by ablation studies to further assess its effectiveness.

## 2. Related Works

### 2.1. Vision Transformer for Medical Image Segmentation

CNN-based techniques like U-Net [32] have notably advanced medical image segmentation by replacing per-image optimization with global function optimization, thus speeding up performance after training. However, CNN-based architectures have limitations in modeling long-range spatial relations due to the intrinsic locality of convolution operations [7, 37]. Although U-Net employs down-sampling and up-sampling techniques, its effective receptive field remains constrained, limiting its capacity to capture long-range dependencies and accommodate significant deformations in medical images. Various enhancements, such as nested U-Net (U-Net++) [50], dilated convolutions [48] and attention mechanisms [29], have been proposed to address these limitations, but advanced CNN-based network architectures for medical image segmentation remain underexplored.

Transformers [38], initially developed for natural language processing tasks, have shown great potential in computer vision. By utilizing the self-attention mechanism, Transformers can capture long-range spatial information, overcoming the limitations of convolutional operations. The ViT was the first purely self-attention-based network applied to images, achieving state-of-the-art performance in image recognition [11]. Unlike convolutional operations, which are constrained by the size of their kernels, transformers possess large receptive fields that enable them to identify correlations among patches, or tokens, across an entire image. The significant success of ViTs in image segmentation has spurred the development of various trans-

former variants, such as the Swin Transformer [28], Pyramid Vision Transformer (PVT) [41], and Convolutional Vision Transformer (CvT) [45], each tailored to enhance segmentation performance further. Transformer-based methods have recently gained traction in medical imaging, particularly for image segmentation tasks, showcasing their ability to effectively model long-range spatial relationships and improve segmentation performance [6, 13, 14, 17, 18].

### 2.2. Large Language Models

The evolution of LLMs began with the pre-training of transformers using masked token prediction, a method that greatly enhances their adaptability across different tasks and modalities, as prominently demonstrated. Building upon this foundation, several models such as GPT [5], Llama [12, 36], and PaLM [8], with their billions of parameters, have exhibited remarkable in-context learning abilities and exceptional performance in zero-shot tasks, including text classification and text infilling [10, 42]. As evidenced by the results in Section 4.3 that show improved performance in medical image segmentation and registration, transformer blocks within these large-scale models possess a unique capability to engage with biomedical data, thereby enhancing a broad range of computer vision tasks.

### 2.3. LLMs for Medical Image Segmentation tasks

In the biomedical imaging field, LLMs have sparked a surge of innovative applications due to their generative potential. Traditional approaches either project visual features directly onto the LLM input layer or use latent bottlenecks to further encode visual tokens [2, 40]. Research has explored the effects of integrating LLM decoders into visual tasks [39], as well as how utilizing LLMs to interpret label features can improve medical image segmentation [24]. Recent studies have demonstrated that incorporating a text-pretrained, frozen LLM block into the encoder of a ViT not only enhances training performance but also boosts accuracy in biomedical image classification tasks [25]. This study underscores the potential of leveraging transformer blocks in LLMs as adaptable encoders for visual data, extending their utility beyond their traditional roles as text embeddings or tokenized output decoders.

## 3. Methodology

### 3.1. Overall Framework Design

The main framework utilizing a frozen layer of a pre-trained LLM for medical image segmentation tasks is illustrated in Figure 1.

Consider a ViT network with an encoder part, denoted as  $V_E$ , which processes the input image  $x$ . This encoder splits the image into patches and applies a patch embedding module. The encoder includes a hybrid attention block, which

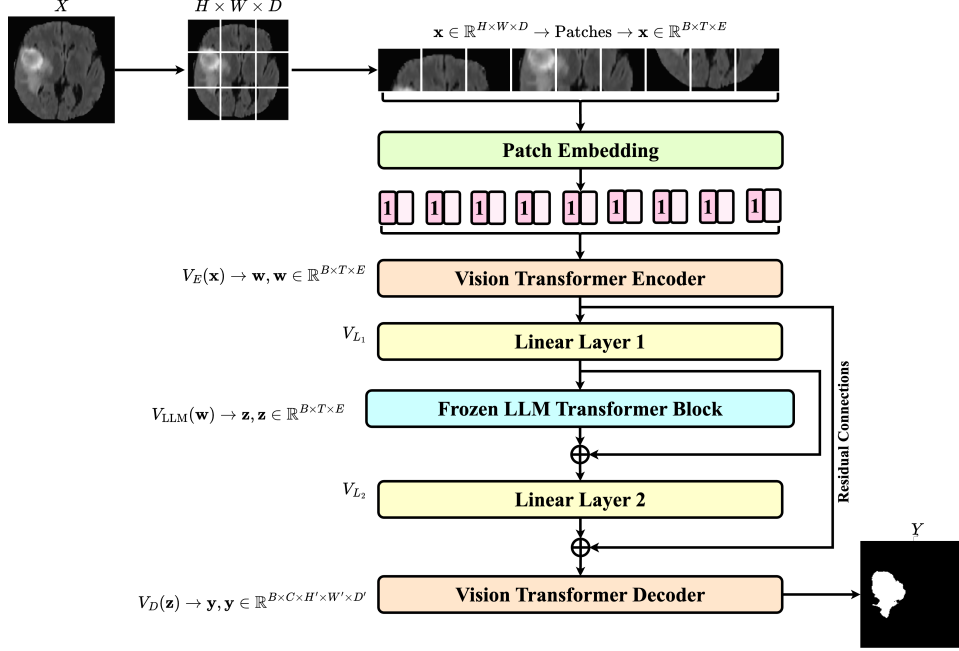


Figure 1. **Overall Framework of the LLM enhanced ViT Model for Medical Image Segmentation.** The architecture integrates a frozen pre-trained LLM transformer block into a Vision Transformer, enhancing feature representation for 3D medical image segmentation with residual connections to improve performance.

plays a crucial role in capturing both global and local contextual information from the image patches. The encoder transforms the input image into a latent representation  $\mathbf{z}$ . The decoder part, denoted as  $V_D$ , reconstructs the latent representation  $\mathbf{z}$  back into the original spatial dimensions to produce the final segmentation map  $\mathbf{y}$ . Thus, the transformation process from the input image to the segmentation output is represented as:

$$V_E(\mathbf{x}) \rightarrow \mathbf{z}, \quad V_D(\mathbf{z}) \rightarrow \mathbf{y} \quad (1)$$

Building upon the foundational ViT network, we enhance its architecture by integrating a frozen transformer block from a pre-trained LLM model, referred to as  $V_{LLM}$ . In this study, we utilize the pre-trained weights from several publicly available LLM models, such as Meta-Llama-3.1-8B [12], Gemma-2-9B [35], Mistral-7B-v0.1 [21], Qwen2-7B [46], and Yi-1.5-9B [47]. These advanced blocks, trained on several billion parameters, are strategically inserted between the encoder  $V_E$  and the decoder  $V_D$ . To align the feature dimensions between  $V_{LLM}$  and  $V_E$ , we introduce two linear layers,  $V_{L1}$  and  $V_{L2}$ , to adapt the dimensions appropriately. Specifically,  $V_{L1}$  is applied just before  $V_{LLM}$  to map the patch embedding output from  $V_E$  to the dimensions required by  $V_{LLM}$ . Following  $V_{LLM}$ ,  $V_{L2}$  re-maps the output from the frozen LLM Transformer block back to the dimensions of the original ViT, allowing the embedded

patches to be converted back to the original spatial dimensions by  $V_D$ . The resulting network can be represented as:

$$V_E(\mathbf{x}) \rightarrow \mathbf{w}, V_{L1} V_{LLM}(\mathbf{w}) V_{L2} \rightarrow \mathbf{z}, V_D(\mathbf{z}) \rightarrow \mathbf{y} \quad (2)$$

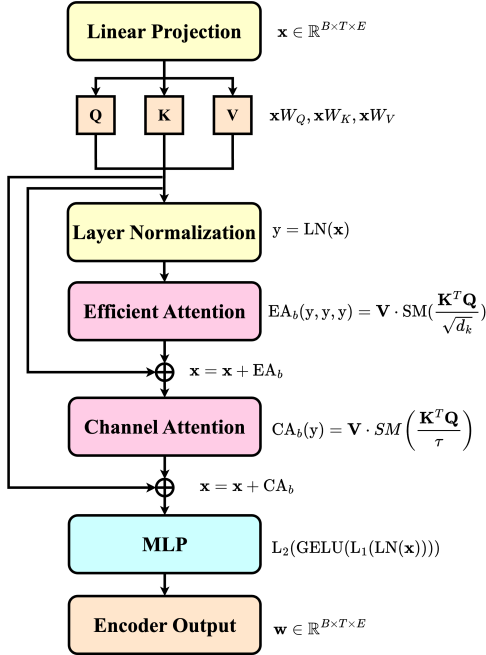
During training, the module  $V_{LLM}$  is kept frozen and is not updated, whereas all other components of the framework, including the linear layers  $V_{L1}$  and  $V_{L2}$ , are trained normally. Additionally, to ensure compatibility with traditional visual backbones, the rotary positional embeddings and attention masks have been removed from  $V_{LLM}$  as discussed in [30].

### 3.2. Vision Transformer Architecture

In this study, we employed a traditional ViT network specifically designed for image segmentation tasks. The process begins with an input image of dimensions  $H \times W \times D$ , where  $H$ ,  $W$ , and  $D$  denote the height, width, and depth of the image, respectively.

Initially, the input image is divided into non-overlapping patches of size  $P \times P \times P$ . Each patch is then transformed into a 1-dimensional vector through a linear embedding layer. This transformation produces a tensor with shape  $(B, T, E)$ , where  $B$  is the batch size,  $T$  is the number of patches, and  $E$  is the embedding size of each patch.

$$\mathbf{x} \in \mathbb{R}^{H \times W \times D} \rightarrow \text{Patches} \rightarrow \mathbf{x} \in \mathbb{R}^{B \times T \times E}$$



Vision Transformer Encoder

Figure 2. **ViT Encoder Block.** The encoder consists of linear projections, followed by layer normalization, efficient attention, channel attention, and an MLP block to produce the output embeddings.

Next, the tensor is processed through a Multiscale Fusion Block with scales of 3, 5 and 7. This block aggregates features from multiple scales, enriching the representation with multi-scale contextual information. Subsequently, the sequence of these multi-scale fused patches is processed through the hybrid attention block within the Transformer encoder. This block integrates Efficient Attention and Channel Attention mechanisms. Efficient Attention captures global dependencies and long-range relationships across patches, while Channel Attention refines feature representations by focusing on the importance of different channels. These combined attention mechanisms enhance the feature extraction process, significantly enriching the tensor’s representations.

The tensor continues to retain its shape of  $(B, T, E)$ , but the feature representations are considerably enhanced by the hybrid attention block. Residual connections are incorporated before and after the hybrid attention block to improve gradient flow and allow embeddings to pass through shortcut paths, enhancing gradient exchange and embedding propagation efficiency [16, 25]. Despite the shape remaining  $(B, T, E)$ , the features are now significantly enriched with advanced contextual information.

$$V_{LLM}(\mathbf{w}) \rightarrow \mathbf{z}, \mathbf{z} \in \mathbb{R}^{B \times T \times E}$$

After processing through the LLM’s Transformer block, the tensor is projected back into the spatial dimensions of the original image. This projection is achieved using a series of up-sampling operations and convolutional layers. The output of this projection stage is a tensor with shape  $(B, C, H', W', D')$ , where  $H'$ ,  $W'$ , and  $D'$  denote the height, width, and depth of the segmentation map, respectively. Here,  $C$  represents the number of output channels, corresponding to the number of classes or segmentation labels.

$$V_D(\mathbf{z}) \rightarrow \mathbf{y}, \mathbf{y} \in \mathbb{R}^{B \times C \times H' \times W' \times D'}$$

In summary, the pipeline involves segmenting the image into patches, embedding these patches into a high-dimensional space, passing them through an LLM Transformer block to capture contextual information, and finally reconstructing the tensor to produce the segmentation map. This segmentation map has spatial dimensions that match the original input image but contains predictions across multiple channels.

## 4. Experiments

### 4.1. Dataset and Preprocessing

To evaluate our results, we used all ten datasets from the Medical Segmentation Decathlon (MSD) challenge [3]. The MSD dataset provides a comprehensive benchmark with 10 diverse medical imaging segmentation tasks, each focusing on different anatomical structures and conditions. It includes annotated images of varying detail and complexity, making it ideal for assessing segmentation performance across multiple scenarios. A summary of the tasks is shown in Table 1.

Task	Modality	Number of Images
Task01_BrainTumour	MRI	484
Task02_Heart	MRI	20
Task03_Liver	CT	100
Task04_Hippocampus	MRI	260
Task05_Prostate	MRI	32
Task06_Lung	CT	53
Task07_Pancreas	CT	281
Task08_HepaticVessel	CT	303
Task09_Spleen	CT	41
Task10_Colon	CT	126

Table 1. Summary of tasks, modalities, and number of images in the MSD dataset.

For each dataset, the data was partitioned into training (70%), validation (20%), and test (approximately 10%) sub-

sets. Data augmentation techniques were applied in cases where the number of images was substantially low to enhance model robustness. The model was implemented in Python using the PyTorch framework and trained on an NVIDIA A100 GPU with 40 GB of memory. We trained the model for 100 epochs with an initial learning rate of  $1 \times 10^{-5}$ , using the Adam optimizer with a batch size of 4. The cross-entropy loss function was employed to train the model for segmentation performance evaluation.

## 4.2. Baselines and comparison metrics

Distinct from current VLMs, our approach operates independently of pre-trained visual encoders and does not use text-based inputs. Unlike traditional VLM models such as SimVLM [43], ViLT [23], FLAVA [34], and CLIP [31], which rely on pre-trained visual encoders for aligning visual features with language, our method is designed to operate effectively without such dependencies. This allows our model to be trained from scratch, focusing exclusively on visual representation learning without the need for language-based inputs, making it versatile for a wider range of visual tasks. A key innovation is our Hybrid Attention Mechanism, combining efficient and channel attention for balanced global and local feature learning, alongside a Multi-Scale Fusion Block that refines precision across different scales [27, 44]. These enhancements enable our model to capture complex visual information and perform detailed segmentation, distinguishing it from traditional VLMs and broadening its applicability beyond vision-language tasks.

Hence, in this study, we compare the training and segmentation performances of the base ViT against the ViT enhanced with different pre-trained LLM transformer blocks across various datasets. To evaluate segmentation performance, we use the Dice Coefficient [9] for overlap accuracy, the 95th percentile of the Hausdorff Distance (HD95) [19] for boundary precision, and the Jaccard Index [20] for similarity measurement. Additionally, we analyze the dice and loss curves to determine how quickly each model stabilizes during training. These metrics collectively provide a comprehensive assessment of the effectiveness and efficiency of the enhanced ViT model.

## 4.3. Quantitative Results

This study evaluates the impact of integrating the pre-trained weights of the Llama 3.1 transformer model [12] as a frozen layer into the existing ViT architecture for medical image segmentation, resulting in the MedVisionLlama model. We compare MedVisionLlama with the baseline ViT model across key metrics, including Dice score, accuracy, precision, recall, Jaccard Index, and HD95 in Section 4.3.1. We also examine the effects on activation maps and training dynamics to assess improvements in feature repre-

sentation and model performance in Section 4.3.2.

### 4.3.1 Comparative Analysis of ViT with MedVisionLlama

The first experiment in this study involved comparing the performance of the base ViT to that of the Llama 3.1-enhanced model across different datasets. The aim was to evaluate the effectiveness of adding a frozen Llama transformer block to training for various medical imaging modalities.

From Table 2, it is evident that integrating the Llama transformer block into the ViT significantly boosts performance across all tasks. The average Dice score improves from 0.74 with ViT to 0.79 with MedVisionLlama, with notable increases of about 0.12 and 0.13 points in Task01 and Task05, respectively. Accuracy rises from 0.93 to 0.96 on average, with Task02 and Task09 showing enhancements of 0.05 points. Precision also improves from 0.68 to 0.76, reflecting better prediction balance, particularly in Task05 and Task09, which see increases of 0.13 and 0.12 points. Recall shows a slight improvement from 0.90 to 0.92 on average, with Task03 and Task09 demonstrating increases of 0.04 points. The Jaccard Index enhances from an average of 0.59 to 0.66, with Task08 and Task09 showing improvements of 0.11 and 0.10 points. Additionally, the Hausdorff Distance at the 95th percentile (HD95) decreases from 15.4 to 11.7, indicating improved boundary alignment, with Task03 and Task06 showing reductions of 5.7 and 5.2 units, respectively. These results collectively highlight the substantial effectiveness of the Llama transformer block in enhancing the ViT’s performance across various medical imaging tasks.

### 4.3.2 Training Performance comparison between ViT and MedVisionLlama

We conducted a critical comparison of training performance between the vanilla ViT and MedVisionLlama models, highlighting the importance of both segmentation accuracy and training curves. Figure 3 demonstrates that the Llama-enhanced ViT outperforms the original ViT in both Dice coefficient and loss metrics across training and validation datasets. MedVisionLlama consistently shows higher Dice scores and lower loss values, indicating improved segmentation accuracy, stability, and faster convergence. This underscores Llama’s effectiveness in enhancing feature representation and overall model performance.

Figure 4 displays the feature activation maps of the ViT and MedVisionLlama models. The top image represents an input MRI slice used for segmentation. The maps show how different features are activated across the input volume at various levels:  $V_E$ ,  $V_{LLM}$ , and  $V_D$ . The ViT model’s activation maps (left column) are more diffuse, indicating broader and less specific feature activations. In contrast, the Med-

Metric	Task01		Task02		Task03		Task04		Task05		Task06		Task07		Task08		Task09		Task10			
+Llama	×	✓	×	✓	×	✓	×	✓	×	✓	×	✓	×	✓	×	✓	×	✓	×	✓	×	✓
Dice	0.72	<b>0.84</b>	0.75	<b>0.78</b>	0.68	<b>0.72</b>	0.71	<b>0.72</b>	0.64	<b>0.77</b>	0.76	<b>0.82</b>	0.82	<b>0.89</b>	0.76	<b>0.78</b>	0.79	<b>0.81</b>	0.75	<b>0.77</b>		
	± 0.14	± <b>0.11</b>	± 0.14	± <b>0.13</b>	± 0.09	± <b>0.08</b>	± 0.12	± <b>0.15</b>	± 0.07	± <b>0.08</b>	± 0.12	± <b>0.10</b>	± 0.11	± <b>0.11</b>	± 0.14	± <b>0.09</b>	± 0.14	± <b>0.13</b>	± 0.10	± <b>0.12</b>		
Accuracy	0.94	<b>0.95</b>	0.88	<b>0.93</b>	0.92	<b>0.94</b>	0.94	<b>0.95</b>	0.95	<b>0.98</b>	0.92	<b>0.95</b>	0.97	<b>0.99</b>	0.91	<b>0.93</b>	0.92	<b>0.97</b>	0.96	<b>0.98</b>		
	± 0.03	± <b>0.01</b>	± 0.04	± <b>0.02</b>	± 0.02	± <b>0.01</b>	± 0.03	± <b>0.02</b>	± 0.03	± <b>0.01</b>	± 0.02	± <b>0.02</b>	± 0.04	± <b>0.01</b>	± 0.03	± <b>0.01</b>	± 0.03	± <b>0.02</b>	± 0.02	± <b>0.01</b>		
Precision	0.70	<b>0.78</b>	0.68	<b>0.74</b>	0.72	<b>0.77</b>	0.68	<b>0.72</b>	0.66	<b>0.79</b>	0.73	<b>0.76</b>	0.69	<b>0.80</b>	0.69	<b>0.74</b>	0.65	<b>0.77</b>	0.63	<b>0.73</b>		
	± 0.04	± <b>0.02</b>	± 0.03	± <b>0.01</b>	± 0.05	± <b>0.02</b>	± 0.04	± <b>0.01</b>	± 0.03	± <b>0.03</b>	± 0.04	± <b>0.02</b>	± 0.05	± <b>0.01</b>	± 0.03	± <b>0.02</b>	± 0.04	± <b>0.01</b>	± 0.03	± <b>0.02</b>		
Recall	0.90	<b>0.91</b>	0.86	<b>0.89</b>	0.88	<b>0.92</b>	0.85	<b>0.88</b>	0.92	<b>0.94</b>	0.87	<b>0.89</b>	0.94	<b>0.96</b>	0.89	<b>0.92</b>	0.90	<b>0.94</b>	0.94	<b>0.95</b>		
	± 0.04	± <b>0.01</b>	± 0.03	± <b>0.02</b>	± 0.04	± <b>0.01</b>	± 0.03	± <b>0.02</b>	± 0.05	± <b>0.03</b>	± 0.02	± <b>0.01</b>	± 0.04	± <b>0.02</b>	± 0.03	± <b>0.01</b>	± 0.04	± <b>0.01</b>	± 0.03	± <b>0.02</b>		
Jaccard	0.54	<b>0.62</b>	0.58	<b>0.64</b>	0.51	<b>0.59</b>	0.61	<b>0.65</b>	0.55	<b>0.62</b>	0.62	<b>0.65</b>	0.66	<b>0.72</b>	0.60	<b>0.71</b>	0.58	<b>0.68</b>	0.63	<b>0.68</b>		
	± 0.05	± <b>0.02</b>	± 0.04	± <b>0.03</b>	± 0.05	± <b>0.01</b>	± 0.04	± <b>0.08</b>	± 0.06	± <b>0.09</b>	± 0.05	± <b>0.11</b>	± 0.09	± <b>0.11</b>	± 0.13	± <b>0.10</b>	± 0.09	± <b>0.13</b>	± 0.08	± <b>0.12</b>		
HD95	14.7	<b>11.2</b>	15.4	<b>12.1</b>	16.5	<b>10.8</b>	15.9	<b>11.6</b>	14.8	<b>12.3</b>	16.2	<b>11.0</b>	15.7	<b>12.0</b>	14.9	<b>11.8</b>	15.6	<b>11.5</b>	14.4	<b>12.2</b>		
	± 3.5	± <b>2.3</b>	± 4.2	± <b>3.1</b>	± 5.1	± <b>2.5</b>	± 4.3	± <b>2.8</b>	± 4.6	± <b>2.6</b>	± 5.2	± <b>2.4</b>	± 4.8	± <b>2.7</b>	± 4.4	± <b>2.5</b>	± 5.0	± <b>2.8</b>	± 4.7	± <b>2.6</b>		

Table 2. Comparison of various metric scores for the ViT (×) and MedVisionLlama (✓) models across Tasks 01 to 10. MedVisionLlama generally outperforms the ViT model in terms of Dice, Accuracy, Precision, Recall, Jaccard, and HD95 scores, indicating improved overall performance and accuracy across different tasks.

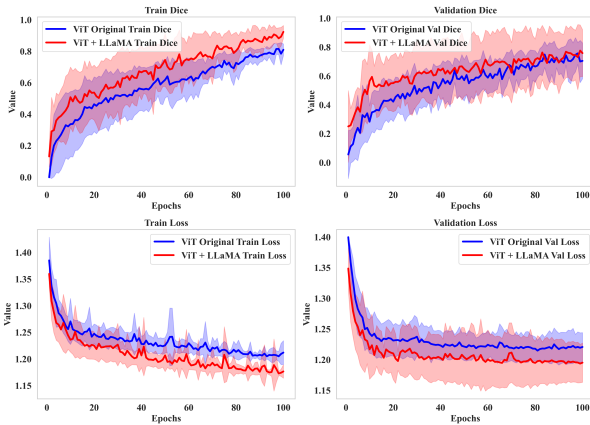


Figure 3. **Training dice and loss curves for ViT and MedVisionLlama.** MedVisionLlama shows higher Dice scores and lower loss compared to the original ViT during training, indicating better segmentation accuracy and faster convergence.

VisionLlama model’s activation maps (right column) exhibit more concentrated and precise activations, particularly around the region of interest. This suggests that incorporating the Llama transformer module enhances the model’s ability to focus on relevant features, thereby improving the accuracy of the segmentation. The improved localization seen in the MedVisionLlama model underscores the effectiveness of LLM-based feature representations in refining segmentation performance.

#### 4.4. Ablation studies

We conducted an ablation study to assess the impact of integrating frozen LLM transformer blocks ( $V_{LLM}$ ), like Llama, into ViT-based segmentation models. In Section

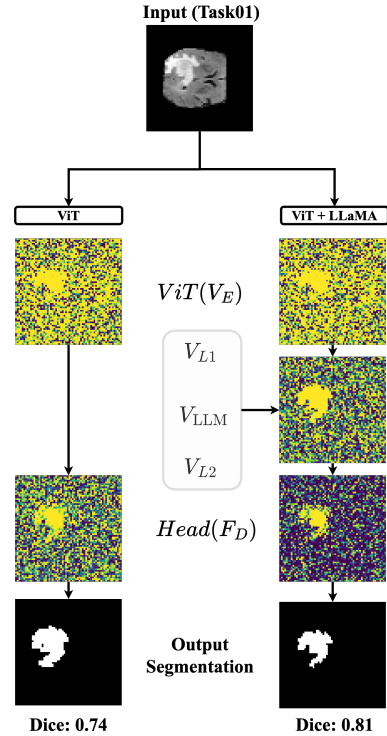


Figure 4. **Comparison of feature activation maps between the ViT and MedVisionLlama models.** MedVisionLlama shows more concentrated and precise feature activations compared to the ViT model, indicating enhanced focus on relevant features and improved segmentation accuracy.

4.4.1, we compare Hybrid Attention (HA) with Spatial Attention (SA) and evaluate Llama against an MLP alternative. In Section 4.3.2, we extend the analysis to include

LLMs like Gemma [35], Mistral [21], Qwen [46], and Yi [47], examining their effects on segmentation accuracy, stability, and the trade-offs between efficiency and complexity.

#### 4.4.1 Model capacity and Fine-tuning

In our initial study, we compare the performance of the ViT enhanced with the Llama model under varying capacities and fine-tuning conditions. Specifically, we evaluate the hybrid attention network against the spatial attention network. Additionally, we introduce a variant model, ViT + MLP, which replaces the Llama layer in the MedVisionLlama model. In the ViT + MLP model, the  $V_{LLM}$  layer between  $V_{L_1}$  and  $V_{L_2}$  is removed and substituted with a GeLU activation function followed by a layer normalization. We performed this study for two datasets, Task01 and Task03.

Model	Params (M)	HA	SA	Task01	Task03
MedVisionLlama	204.48	×	✓	0.79 ± 0.04	0.71 ± 0.07
MedVisionLlama	218.12	✓	×	<b>0.84</b> ± <b>0.05</b>	<b>0.72</b> ± <b>0.07</b>
ViT	0.84	✓	×	0.72 ± 0.08	0.68 ± 0.05
ViT + MLP	0.96	✓	×	0.74 ± 0.06	0.65 ± 0.11
MedVisionLlama	218.12	✓	×	<b>0.84</b> ± <b>0.05</b>	<b>0.72</b> ± <b>0.07</b>

Table 3. Comparison of different models across various metrics. HA: Hybrid Attention, SA: Spatial Attention. The MedVisionLlama model with HA and SA shows superior performance in Task01 and Task03 Dice scores compared to other configurations, emphasizing its effectiveness in enhancing segmentation accuracy.

Evaluating models with HA versus SA reveals that HA consistently provides superior performance and stability. For example, in Task01, MedVisionLlama with HA shows a notable improvement in Dice score compared to SA, and a similar trend is observed in Task03. This suggests that HA offers higher accuracy and reduced variability in performance. Additionally, the Llama block outperforms both the MLP and Vanilla ViT models, achieving the highest Dice scores across tasks. Specifically, MedVisionLlama shows superior performance, surpassing both the ViT and ViT + MLP models. This indicates that the Llama block enhances model performance and consistency compared to the other approaches.

#### 4.4.2 Comparison with several pre-trained LLMs

In the second study, we assessed the impact of integrating several publicly available pre-trained frozen LLM transformer blocks into the ViT model. This evaluation was conducted by comparing these enhanced models against a base-

line vanilla ViT. For this analysis, the Dice score was used as the sole metric to assess segmentation performance. We examined the impact of five different LLMs across multiple datasets. The outcomes of this comparison are detailed in Table 4, highlighting the relative performance improvements brought about by each LLM when integrated into the ViT framework.

From Table 4, it can be seen that the models Qwen and Yi consistently deliver strong performance across all 10 tasks, often achieving some of the highest Dice scores. For instance, in Task01, Yi outperforms with a Dice score of 0.86, while Qwen follows closely with 0.82. Similarly, in Task07, Qwen achieves a score of 0.76, surpassing Yi’s 0.73. These results demonstrate the superior performance of Qwen and Yi across various medical imaging tasks. Conversely, the base ViT model shows the lowest performance across most tasks, with significantly lower scores compared to the other models. For example, in Task06, the ViT model only achieves a score of 0.76, while Qwen and Yi reach higher scores of 0.83 and 0.86, respectively. Gemma, Llama, and Mistral exhibit moderate performance, generally outperforming the ViT model but not quite reaching the levels of Qwen and Yi. For instance, in Task09, Gemma scores 0.77, Llama scores 0.81, and Mistral scores 0.85, which are higher than ViT’s 0.79 but slightly lower than Yi’s 0.86.

Task	ViT	ViT + Gemma	ViT + Llama	ViT + Mistral	ViT + Qwen	ViT + Yi
Params (M)	0.84	264.25	218.12	218.12	233.06	202.39
Task01	0.72 ± 0.14	0.77 ± 0.12	0.84 ± 0.11	0.74 ± 0.13	0.82 ± 0.13	<b>0.86</b> ± <b>0.12</b>
Task02	0.75 ± 0.14	0.73 ± 0.08	0.78 ± 0.13	<b>0.79</b> ± <b>0.14</b>	± 0.76 ± 0.13	<b>0.79</b> ± <b>0.12</b>
Task03	0.68 ± 0.09	0.75 ± 0.08	0.72 ± 0.11	0.65 ± 0.12	<b>0.76</b> ± <b>0.13</b>	0.73 ± 0.10
Task04	0.71 ± 0.11	0.72 ± 0.12	0.72 ± 0.10	0.69 ± 0.13	<b>0.78</b> ± <b>0.13</b>	0.77 ± 0.10
Task05	0.64 ± 0.07	0.73 ± 0.08	0.77 ± 0.08	0.81 ± 0.09	<b>0.83</b> ± <b>0.07</b>	0.79 ± 0.09
Task06	0.76 ± 0.12	0.79 ± 0.14	0.82 ± 0.10	0.75 ± 0.10	0.83 ± 0.13	<b>0.86</b> ± <b>0.12</b>
Task07	0.82 ± 0.11	0.83 ± 0.08	<b>0.89</b> ± <b>0.11</b>	0.82 ± 0.05	0.87 ± 0.07	0.88 ± 0.10
Task08	0.76 ± 0.14	0.80 ± 0.13	0.78 ± 0.09	<b>0.81</b> ± <b>0.08</b>	0.73 ± 0.10	0.77 ± 0.12
Task09	0.79 ± 0.14	0.77 ± 0.12	0.81 ± 0.13	0.85 ± 0.10	0.83 ± 0.13	<b>0.86</b> ± <b>0.11</b>
Task10	0.75 ± 0.12	0.75 ± 0.10	0.77 ± 0.12	0.74 ± 0.13	0.80 ± 0.13	<b>0.83</b> ± <b>0.09</b>

Table 4. Comparison of segmentation performance across different LLM models for each task based on Dice score. The ViT + Yi model consistently achieves high Dice scores across various tasks compared to other models, demonstrating its superior effectiveness in improving segmentation accuracy.

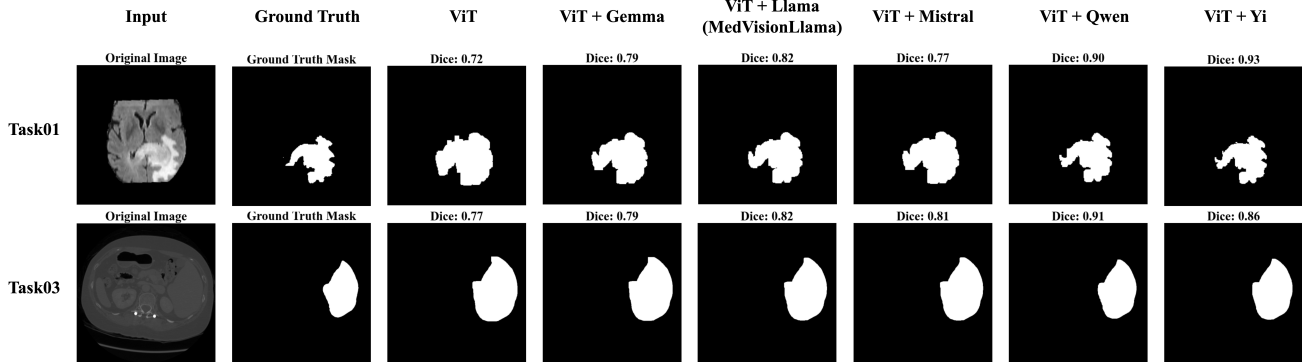


Figure 5. Segmentation results of different pre-trained LLM transformer blocks on Task01 and Task03. The Dice scores displayed above the segmentation results highlight that lighter LLMs like Yi and Qwen achieve higher scores compared to other heavier models.

Figure 5 demonstrates the segmentation performance of different pre-trained LLM transformer blocks, specifically for Task01 and Task03. Each model’s Dice coefficient, a metric that quantifies the similarity between predicted and ground truth masks, is displayed. From the results, it is evident that ViT + Yi and ViT + Qwen configurations consistently achieve high Dice scores across both tasks, indicating superior segmentation accuracy. On the other hand, the vanilla ViT model without additional LLM enhancements shows the lowest performance, emphasizing the importance of integrating these advanced LLM-based blocks for improved segmentation.

This comparison underscores the advantage of incorporating advanced LLMs which significantly enhance segmentation performance in various medical imaging tasks. Lighter models such as Qwen and Yi often benefit from faster training times and lower inference costs, making them ideal for tasks that do not require the extensive representational capacity of larger models. In contrast, while heavier models like Gemma, Llama, and Mistral offer greater capacity and may perform exceptionally well in more complex scenarios, they may be excessive for simpler segmentation tasks. This suggests that for specific medical imaging applications, the efficiency and speed of lighter models can be more advantageous than the increased complexity of larger models, highlighting the importance of choosing the right model size based on the task’s demands.

## 5. Discussion and Conclusion

In this study, we explored the novel integration of a frozen transformer block from pre-trained LLMs into the encoder of a ViT-based medical image segmentation model. This approach led to significant enhancements in both performance and accuracy across various medical imaging modalities. Additionally, we proposed an innovative Hybrid Attention Mechanism that effectively balances global and

local feature learning by combining efficient and channel attention, alongside a Multi-Scale Fusion Block designed to aggregate features across multiple scales, further refining segmentation precision. Our extensive evaluation, including ablation studies, demonstrated the efficacy of incorporating LLM transformer blocks, highlighting their potential to substantially elevate the accuracy and robustness of medical image segmentation models.

Integrating the pre-trained weights of the Llama 3.1 transformer block into the ViT model significantly enhances segmentation accuracy and stability across medical imaging tasks. This integration leads to improved key metrics like Dice score, precision, and Jaccard Index, with more precise activations and better feature representation. Ablation studies confirm that frozen LLM transformer blocks, such as Llama, combined with the hybrid attention block, consistently outperform alternative configurations, offering superior segmentation performance.

Moreover, advanced LLMs like Qwen and Yi demonstrate substantial performance gains, often surpassing heavier models like Llama and Mistral, emphasizing the importance of balancing model efficiency with task complexity. A possible hypothesis for this trend is that Qwen and Yi incorporate unique architectural enhancements and optimizations that effectively strike a balance between computational efficiency and representation power. Unlike the heavier models, which offer high feature representation capabilities at the cost of increased computational load and potential overfitting, Qwen and Yi likely utilize advanced mechanisms that are better aligned with the specific needs of medical imaging tasks. Through this study, we demonstrate that although LLMs are primarily trained on textual data, they can act as powerful enhancers for image segmentation tasks, providing significant boosts to performance and enabling more accurate and stable outcomes in medical imaging applications.



## References

- [1] Abdelrahman Abdelhamed, Mahmoud Afifi, and Alec Go. What do you see? enhancing zero-shot image classification with multimodal large language models. *arXiv preprint arXiv:2405.15668*, 2024. 1
- [2] Jean-Baptiste Alayrac, Jeff Donahue, Pauline Luc, Antoine Miech, Iain Barr, Yana Hasson, Karel Lenc, Arthur Mensch, Katherine Millican, Malcolm Reynolds, et al. Flamingo: a visual language model for few-shot learning. *Advances in neural information processing systems*, 35:23716–23736, 2022. 2
- [3] Michela Antonelli, Annika Reinke, Spyridon Bakas, Keyvan Farahani, Annette Kopp-Schneider, Bennett A Landman, Geert Litjens, Bjoern Menze, Olaf Ronneberger, Ronald M Summers, et al. The medical segmentation decathlon. *Nature communications*, 13(1):4128, 2022. 4
- [4] Reza Azad, Amirhossein Kazerouni, Moein Heidari, Ehsan Khodapanah Aghdam, Amirali Molaei, Yiwei Jia, Abin Jose, Rijo Roy, and Dorit Merhof. Advances in medical image analysis with vision transformers: a comprehensive review. *Medical Image Analysis*, page 103000, 2023. 1
- [5] Tom Brown, Benjamin Mann, Nick Ryder, Melanie Subbiah, Jared D Kaplan, Prafulla Dhariwal, Arvind Neelakantan, Pranav Shyam, Girish Sastry, Amanda Askell, et al. Language models are few-shot learners. *Advances in neural information processing systems*, 33:1877–1901, 2020. 2
- [6] Hu Cao, Yueyue Wang, Joy Chen, Dongsheng Jiang, Xiaopeng Zhang, Qi Tian, and Manning Wang. Swin-unet: Unet-like pure transformer for medical image segmentation. In *European conference on computer vision*, pages 205–218. Springer, 2022. 2
- [7] Jieneng Chen, Yongyi Lu, Qihang Yu, Xiangde Luo, Ehsan Adeli, Yan Wang, Le Lu, Alan L Yuille, and Yuyin Zhou. Transunet: Transformers make strong encoders for medical image segmentation. *arXiv preprint arXiv:2102.04306*, 2021. 2
- [8] Aakanksha Chowdhery, Sharan Narang, Jacob Devlin, Maarten Bosma, Gaurav Mishra, Adam Roberts, Paul Barham, Hyung Won Chung, Charles Sutton, Sebastian Gehrmann, et al. Palm: Scaling language modeling with pathways. *Journal of Machine Learning Research*, 24(240):1–113, 2023. 2
- [9] L. R. Dice. Measures of the amount of ecologic association between species. *Ecology*, 26(3):297–302, 1945. 5
- [10] Chris Donahue, Mina Lee, and Percy Liang. Enabling language models to fill in the blanks. *arXiv preprint arXiv:2005.05339*, 2020. 2
- [11] Alexey Dosovitskiy, Lucas Beyer, Alexander Kolesnikov, Dirk Weissenborn, Xiaohua Zhai, Thomas Unterthiner, Mostafa Dehghani, Matthias Minderer, Georg Heigold, Sylvain Gelly, et al. An image is worth 16x16 words: Transformers for image recognition at scale. *arXiv preprint arXiv:2010.11929*, 2020. 1, 2
- [12] Abhimanyu Dubey, Abhinav Jauhri, Abhinav Pandey, Abhishek Kadian, Ahmad Al-Dahle, Aiesha Letman, Akhil Mathur, Alan Schelten, Amy Yang, Angela Fan, et al. The llama 3 herd of models. *arXiv preprint arXiv:2407.21783*, 2024. 2, 3, 5
- [13] Sina Ghorbani Kolahi, Seyed Kamal Chaharsooghi, Toktam Khatibi, Afshin Bozorgpour, Reza Azad, Moein Heidari, Ilker Hacihaliloglu, and Dorit Merhof. Msa2net: Multi-scale adaptive attention-guided network for medical image segmentation. *arXiv e-prints*, pages arXiv–2407, 2024. 2
- [14] Ali Hatamizadeh, Yucheng Tang, Vishwesh Nath, Dong Yang, Andriy Myronenko, Bennett Landman, Holger R Roth, and Daguang Xu. Unetr: Transformers for 3d medical image segmentation. In *Proceedings of the IEEE/CVF winter conference on applications of computer vision*, pages 574–584, 2022. 2
- [15] Kelei He, Chen Gan, Zhuoyuan Li, Islem Rekik, Zihao Yin, Wen Ji, Yang Gao, Qian Wang, Junfeng Zhang, and Ding-gang Shen. Transformers in medical image analysis. *Intelligent Medicine*, 3(1):59–78, 2023. 1
- [16] Kaiming He, Xiangyu Zhang, Shaoqing Ren, and Jian Sun. Deep residual learning for image recognition. In *Proceedings of the IEEE conference on computer vision and pattern recognition*, pages 770–778, 2016. 4
- [17] Moein Heidari, Amirhossein Kazerouni, Milad Soltany, Reza Azad, Ehsan Khodapanah Aghdam, Julien Cohen-Adad, and Dorit Merhof. Hiformer: Hierarchical multi-scale representations using transformers for medical image segmentation. In *Proceedings of the IEEE/CVF winter conference on applications of computer vision*, pages 6202–6212, 2023. 2
- [18] Xiaohong Huang, Zhifang Deng, Dandan Li, and Xueguang Yuan. Missformer: An effective medical image segmentation transformer. *arXiv preprint arXiv:2109.07162*, 2021. 2
- [19] Daniel P. Huttenlocher, Gary A. Klanderman, and W. J. Rucklidge. Comparing images using the hausdorff distance. *IEEE Transactions on Pattern Analysis and Machine Intelligence*, 15(9):850–863, 1993. 5
- [20] Paul Jaccard. Étude comparative de la distribution florale dans une portion des alpes et des pyrénées. *Bulletin de la Société Vaudoise des Sciences Naturelles*, 37:547–579, 1901. 5
- [21] Albert Q Jiang, Alexandre Sablayrolles, Arthur Mensch, Chris Bamford, Devendra Singh Chaplot, Diego de las Casas, Florian Bressand, Gianna Lengyel, Guillaume Lample, Lucile Saulnier, et al. Mistral 7b. *arXiv preprint arXiv:2310.06825*, 2023. 3, 7
- [22] Pravneet Kaur, Gautam Siddharth Kashyap, Ankit Kumar, Md Tabrez Nafis, Sandeep Kumar, and Vikrant Shokeen. From text to transformation: A comprehensive review of large language models’ versatility. *arXiv preprint arXiv:2402.16142*, 2024. 1
- [23] Wonjae Kim, Bokyung Son, and Ildoo Kim. Vilt: Vision-and-language transformer without convolution or region supervision. In *International conference on machine learning*, pages 5583–5594. PMLR, 2021. 5
- [24] Suruchi Kumari, Aryan Das, Swalpa Kumar Roy, Indu Joshi, and Pravendra Singh. Leveraging task-specific knowledge from llm for semi-supervised 3d medical image segmentation. *arXiv preprint arXiv:2407.05088*, 2024. 2

- [25] Zhixin Lai, Jing Wu, Suiyao Chen, Yucheng Zhou, and Naira Hovakimyan. Residual-based language models are free boosters for biomedical imaging tasks. In *Proceedings of the IEEE/CVF Conference on Computer Vision and Pattern Recognition*, pages 5086–5096, 2024. 1, 2, 4
- [26] Zihan Li, Yunxiang Li, Qingde Li, Puyang Wang, Dazhuo Guo, Le Lu, Dakai Jin, You Zhang, and Qingqi Hong. Lvit: language meets vision transformer in medical image segmentation. *IEEE transactions on medical imaging*, 2023. 1
- [27] Tsung-Yi Lin, Piotr Dollár, Ross Girshick, Kaiming He, Bharath Hariharan, and Serge Belongie. Feature pyramid networks for object detection. In *Proceedings of the IEEE conference on computer vision and pattern recognition*, pages 2117–2125, 2017. 5
- [28] Ze Liu, Yutong Lin, Yue Cao, Han Hu, Yixuan Wei, Zheng Zhang, Stephen Lin, and Baining Guo. Swin transformer: Hierarchical vision transformer using shifted windows. In *Proceedings of the IEEE/CVF international conference on computer vision*, pages 10012–10022, 2021. 2
- [29] Ozan Oktay, Jo Schlemper, Loic Le Folgoc, Matthew Lee, Mattias Heinrich, Kazunari Misawa, Kensaku Mori, Steven McDonagh, Nils Y Hammerla, Bernhard Kainz, et al. Attention u-net: Learning where to look for the pancreas. *arXiv preprint arXiv:1804.03999*, 2018. 2
- [30] Ziqi Pang, Ziyang Xie, Yunze Man, and Yu-Xiong Wang. Frozen transformers in language models are effective visual encoder layers. *arXiv preprint arXiv:2310.12973*, 2023. 1, 3
- [31] Alec Radford, Jong Wook Kim, Chris Hallacy, Aditya Ramesh, Gabriel Goh, Sandhini Agarwal, Girish Sastry, Amanda Askell, Pamela Mishkin, Jack Clark, et al. Learning transferable visual models from natural language supervision. In *International conference on machine learning*, pages 8748–8763. PMLR, 2021. 1, 5
- [32] Olaf Ronneberger, Philipp Fischer, and Thomas Brox. U-net: Convolutional networks for biomedical image segmentation. In *Medical image computing and computer-assisted intervention—MICCAI 2015: 18th international conference, Munich, Germany, October 5–9, 2015, proceedings, part III 18*, pages 234–241. Springer, 2015. 2
- [33] Gordon D Schiff, Seijeoung Kim, Richard Abrams, Karen Cosby, Bruce Lambert, Arthur S Elstein, Scott Hasler, Nela Krosnjak, Richard Odwazny, Mary F Wisniewski, et al. Diagnosing diagnosis errors: lessons from a multi-institutional collaborative project. *Advances in patient safety: from research to implementation (volume 2: concepts and methodology)*, 2005. 1
- [34] Amanpreet Singh, Ronghang Hu, Vedanuj Goswami, Guillaume Couairon, Wojciech Galuba, Marcus Rohrbach, and Douwe Kiela. Flava: A foundational language and vision alignment model. In *Proceedings of the IEEE/CVF Conference on Computer Vision and Pattern Recognition*, pages 15638–15650, 2022. 5
- [35] Gemma Team, Morgane Riviere, Shreya Pathak, Pier Giuseppe Sessa, Cassidy Hardin, Surya Bhupatiraju, Léonard Hussenot, Thomas Mesnard, Bobak Shahriari, Alexandre Ramé, et al. Gemma 2: Improving open language models at a practical size. *arXiv preprint arXiv:2408.00118*, 2024. 3, 7
- [36] Hugo Touvron, Thibaut Lavril, Gautier Izacard, Xavier Martinet, Marie-Anne Lachaux, Timothée Lacroix, Baptiste Rozière, Naman Goyal, Eric Hambro, Faisal Azhar, et al. Llama: Open and efficient foundation language models. *arXiv preprint arXiv:2302.13971*, 2023. 2
- [37] Jeya Maria Jose Valanarasu, Poojan Oza, Ilker Hacihaliloglu, and Vishal M Patel. Medical transformer: Gated axial-attention for medical image segmentation. In *Medical image computing and computer assisted intervention—MICCAI 2021: 24th international conference, Strasbourg, France, September 27–October 1, 2021, proceedings, part I 24*, pages 36–46. Springer, 2021. 2
- [38] Ashish Vaswani, Noam Shazeer, Niki Parmar, Jakob Uszkoreit, Llion Jones, Aidan N Gomez, Łukasz Kaiser, and Illia Polosukhin. Attention is all you need. *Advances in neural information processing systems*, 30, 2017. 2
- [39] Jiahao Wang, Wenqi Shao, Mengzhao Chen, Chengyue Wu, Yong Liu, Kaipeng Zhang, Songyang Zhang, Kai Chen, and Ping Luo. Adapting llama decoder to vision transformer. *arXiv preprint arXiv:2404.06773*, 2024. 2
- [40] Wenhai Wang, Zhe Chen, Xiaokang Chen, Jiannan Wu, Xizhou Zhu, Gang Zeng, Ping Luo, Tong Lu, Jie Zhou, Yu Qiao, et al. Visionllm: Large language model is also an open-ended decoder for vision-centric tasks. *Advances in Neural Information Processing Systems*, 36, 2024. 2
- [41] Wenhai Wang, Enze Xie, Xiang Li, Deng-Ping Fan, Kaitao Song, Ding Liang, Tong Lu, Ping Luo, and Ling Shao. Pyramid vision transformer: A versatile backbone for dense prediction without convolutions. In *Proceedings of the IEEE/CVF international conference on computer vision*, pages 568–578, 2021. 2
- [42] Zhiqiang Wang, Yiran Pang, and Yanbin Lin. Large language models are zero-shot text classifiers. *arXiv preprint arXiv:2312.01044*, 2023. 2
- [43] Zirui Wang, Jiahui Yu, Adams Wei Yu, Zihang Dai, Yulia Tsvetkov, and Yuan Cao. Simvlm: Simple visual language model pretraining with weak supervision. *arXiv preprint arXiv:2108.10904*, 2021. 5
- [44] Sanghyun Woo, Jongchan Park, Joon-Young Lee, and In So Kweon. Cbam: Convolutional block attention module. In *Proceedings of the European conference on computer vision (ECCV)*, pages 3–19, 2018. 5
- [45] Haiping Wu, Bin Xiao, Noel Codella, Mengchen Liu, Xiyang Dai, Lu Yuan, and Lei Zhang. Cvt: Introducing convolutions to vision transformers. In *Proceedings of the IEEE/CVF international conference on computer vision*, pages 22–31, 2021. 2
- [46] An Yang, Baosong Yang, Binyuan Hui, Bo Zheng, Bowen Yu, Chang Zhou, Chengpeng Li, Chengyuan Li, Dayiheng Liu, Fei Huang, et al. Qwen2 technical report. *arXiv preprint arXiv:2407.10671*, 2024. 3, 7
- [47] Alex Young, Bei Chen, Chao Li, Chengen Huang, Ge Zhang, Guanwei Zhang, Heng Li, Jiangcheng Zhu, Jianqun Chen, Jing Chang, et al. Yi: Open foundation models by 01. ai. *arXiv preprint arXiv:2403.04652*, 2024. 3, 7

- [48] Fisher Yu and Vladlen Koltun. Multi-scale context aggregation by dilated convolutions. *arXiv preprint arXiv:1511.07122*, 2015. [2](#)
- [49] Sukmin Yun, Seong Hyeon Park, Paul Hongsuck Seo, and Jinwoo Shin. Ifseg: Image-free semantic segmentation via vision-language model. In *Proceedings of the IEEE/CVF Conference on Computer Vision and Pattern Recognition*, pages 2967–2977, 2023. [1](#)
- [50] Zongwei Zhou, Md Mahfuzur Rahman Siddiquee, Nima Tajbakhsh, and Jianming Liang. Unet++: A nested u-net architecture for medical image segmentation. In *Deep Learning in Medical Image Analysis and Multimodal Learning for Clinical Decision Support: 4th International Workshop, DLMIA 2018, and 8th International Workshop, ML-CDS 2018, Held in Conjunction with MICCAI 2018, Granada, Spain, September 20, 2018, Proceedings 4*, pages 3–11. Springer, 2018. [2](#)

## Supplementary Material

The supplementary material provides a comprehensive examination of various aspects of attention strategies, model performance, and computational complexity in medical image segmentation. [Appendix A](#) compares three hybrid attention strategies—Sequential, Parallel, and Interleaved—highlighting their parameter counts and segmentation performance on two tasks. The Sequential strategy emerges as the most balanced approach in terms of performance and complexity. [Appendix B](#) details the performance of Vision Transformer (ViT) and ViT + Llama models across different input sizes, demonstrating that while Llama increases training time, it significantly enhances segmentation accuracy, particularly at higher resolutions. [Appendix C](#) features visual comparisons of different segmentation results, providing insights into the effectiveness and alignment capabilities of different LLMs. In [Appendix D](#), we evaluate different ViT models integrated with LLMs, revealing that the ViT + Yi model achieves the highest Dice score and lowest HD95 with the fewest parameters. This suggests that advanced LLMs like Yi and Llama enhance model performance while maintaining efficiency. Overall, these appendices underscore the impact of hybrid attention strategies, input sizes, and LLM integrations on segmentation accuracy and computational efficiency.

### Appendix A. Hybrid Attention Block Strategy

This comparison focuses on three hybrid attention strategies—Sequential, Parallel, and Interleaved—assessing their model complexity (in terms of parameters) and segmentation performance (measured by Dice scores) on two tasks, Task01 and Task03 as shown in [Figure 1](#). From [Table 1](#), the Sequential strategy has 54.2 million parameters and delivers the best results, with a Task01 Dice score of 0.85 and a Task03 Dice score of 0.78, indicating strong segmentation performance while maintaining a moderate parameter count. The Parallel strategy, designed to run efficient attention and channel attention simultaneously, uses fewer parameters (52.3 million), but sacrifices performance, achieving a Task01 Dice score of 0.80 and a Task03 Dice score of 0.72, suggesting that the reduced complexity affects its ability to capture task-relevant features effectively. The Interleaved strategy, which alternates between attention mechanisms, has the highest parameter count at 62.7 million, but its performance is somewhat in between, with a Task01 Dice score of 0.82 and a Task03 Dice score of 0.75. This shows that increasing parameters doesn't necessarily lead to improved performance over the simpler Sequential strategy. Overall, the Sequential strategy strikes the best balance between model complexity and performance, especially for Task01, whereas the Parallel strategy trades off performance for a lower parameter count. The Interleaved strategy, despite being the most complex, does not significantly

cantly outperform the other approaches.

Attention Strategy	Params (M)	Task01 Dice	Task03 Dice
Sequential	54.2	$0.85 \pm 0.02$	$0.78 \pm 0.03$
Parallel	52.3	$0.80 \pm 0.04$	$0.72 \pm 0.05$
Interleaved	62.7	$0.82 \pm 0.03$	$0.75 \pm 0.04$

Table 1. Comparison of hybrid attention strategies in terms of parameters (in millions) and segmentation performance (Dice scores) on Task01 and Task03.

### Appendix B. Input Size, Training Time, and Accuracy

[Table 2](#) compares the performance of two models, ViT and ViT + Llama, across different input sizes for medical image segmentation tasks. The input resolutions examined are  $64 \times 64 \times 40$ ,  $128 \times 128 \times 80$ , and  $240 \times 240 \times 156$  (original resolution), with the metrics being training time (in hours) and Dice score, which reflects segmentation accuracy.

For the smallest input size ( $64 \times 64 \times 40$ ), the ViT model has a training time of 1.27 hours and a Dice score of  $0.65 \pm 0.05$ . When combined with Llama, the training time increases slightly to 1.52 hours, but the Dice score improves to  $0.70 \pm 0.04$ . At a medium input size ( $128 \times 128 \times 80$ ), ViT requires 3.18 hours to train and achieves a Dice score of  $0.75 \pm 0.03$ . The ViT + Llama model takes 4.21 hours but increases the Dice score to  $0.80 \pm 0.03$ . For the largest, original resolution ( $240 \times 240 \times 156$ ), ViT takes 7.54 hours to train and results in a Dice score of  $0.79 \pm 0.02$ . Adding Llama increases the training time to 9.15 hours, but further improves the Dice score to  $0.83 \pm 0.02$ .

Across all input sizes, the ViT + Llama model consistently outperforms the standalone ViT model in terms of Dice score, indicating that Llama enhances the model's ability to segment images more accurately. Integrating Llama increases the training time at each input size, but the performance gains suggest that the additional time is justified, especially for higher resolution images where segmentation accuracy is more critical. As input size increases, both models require more training time, and Dice scores improve. However, the relative improvement from adding Llama becomes more pronounced at higher resolutions, suggesting that Llama might better capture complex features in detailed images. For the  $64 \times 64 \times 40$  input size, the improvement in Dice score when using Llama is modest (0.65 to 0.70), whereas for the largest input size, the improvement is more significant (0.79 to 0.83). Thus, the ViT + Llama model seems particularly beneficial at higher resolutions where the quality of segmentation is more important.

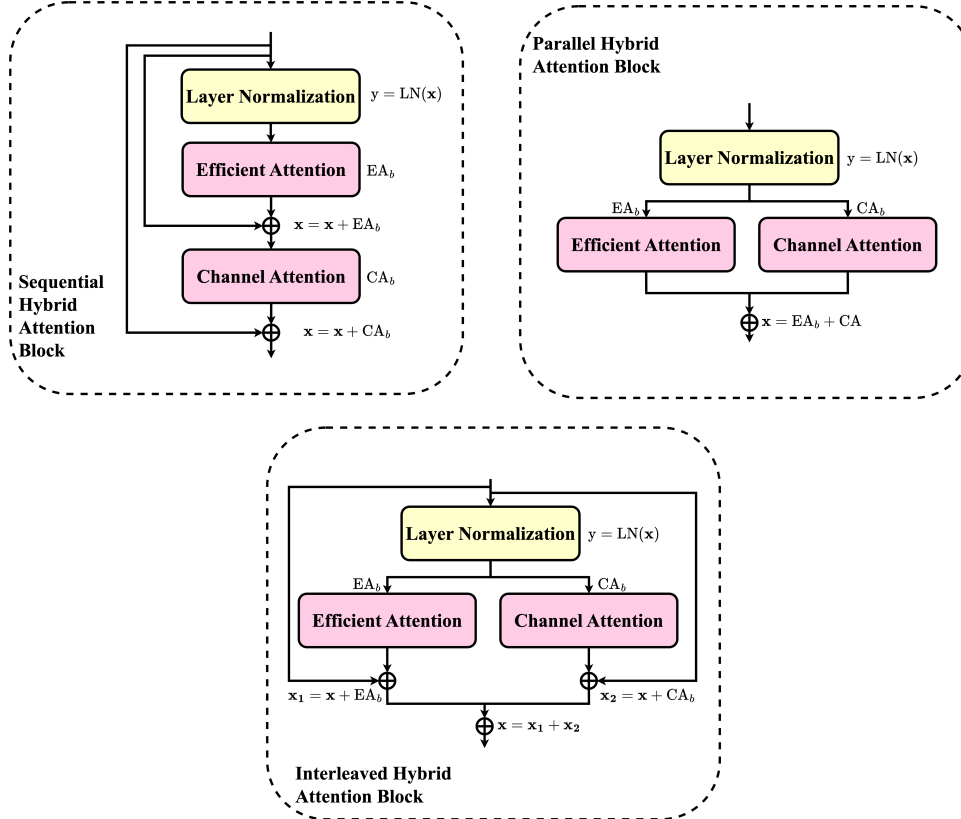


Figure 1. **Comparison of Hybrid Attention Strategies.** Sequential, Parallel, and Interleaved strategies are compared by parameter counts and Dice scores, with Sequential offering the best performance-to-complexity balance.

Model	$64 \times 64 \times 40$		$128 \times 128 \times 80$		$240 \times 240 \times 156$	
	TT	DSC	TT	DSC	TT	DSC
ViT	1.27	$0.65 \pm 0.05$	3.18	$0.75 \pm 0.03$	7.54	$0.79 \pm 0.02$
ViT + Llama	1.52	$0.70 \pm 0.04$	4.21	$0.80 \pm 0.03$	9.15	$0.83 \pm 0.02$

Table 2. Training time and Dice score comparison between ViT and ViT + Llama for different input sizes. TT: Training Time (In hours), DSC: Dice Score

## Appendix C. Further Visualization Results

Figure 2 provides a visual comparison of segmentation performance across various tasks of the MSD dataset using six different models. For each task, the segmentation results are displayed along with their corresponding Dice scores. It is evident that models incorporating LLM-based pre-trained transformers, such as ViT + Llama and ViT + Yi, outperform the baseline ViT model. Visually, these models exhibit more precise segmentations, capturing the target regions more accurately compared to the vanilla ViT model. Quantitatively, the Dice scores for the LLM-enhanced models are consistently higher, confirming the advantage of leveraging pre-trained layers from LLMs for medical im-

age segmentation. This highlights the impact of incorporating LLM transformers into the ViT architecture, leading to better overall segmentation performance.

## Appendix D. Computational Complexity

Table 3 evaluates the performance and computational complexity of different ViT models integrated with various Large Language Models (LLMs) and methods on Task01. The results show that the ViT + Yi model achieves the highest Dice score of 0.86 and the lowest Hausdorff Distance at the 95th percentile (HD95) of 7.9, demonstrating superior accuracy and boundary alignment with the fewest parameters (202.39 million). This indicates that incorporating the Yi LLM effectively enhances segmentation performance

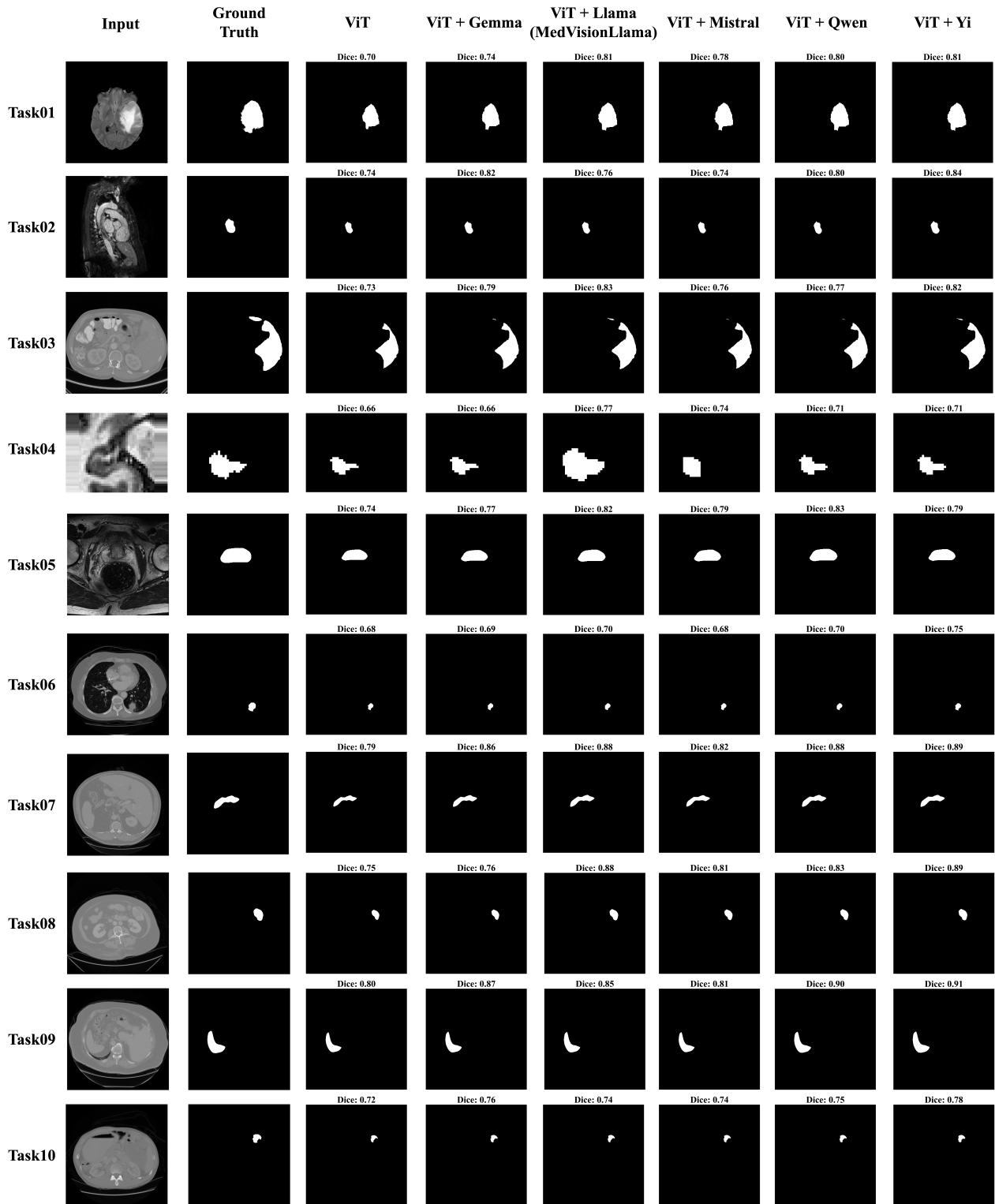


Figure 2. **Segmentation Comparison Across MSD Tasks.** This figure compares six models, with LLM-enhanced models like ViT + Llama and ViT + Yi showing more precise segmentations and higher Dice scores than the baseline ViT, highlighting the benefits of using pre-trained LLM transformers.

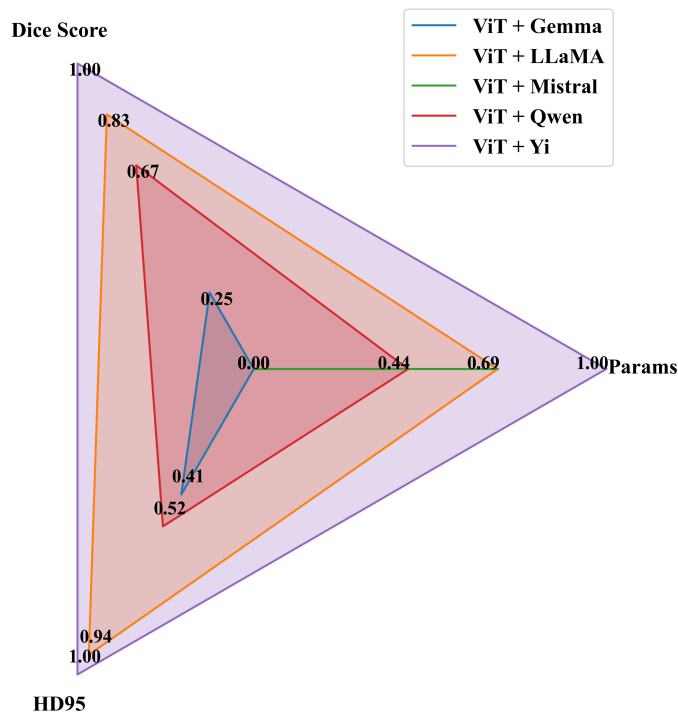


Figure 3. **Radar chart comparing segmentation metrics.** Llama and Yi show high Dice scores and low HD95 values, with Yi excelling in performance and efficiency.

Model	Params (M)	Task01 Dice	Task01 HD95
ViT	0.84	$0.72 \pm 0.14$	$12.5 \pm 3.6$
ViT + Gemma	264.25	$0.77 \pm 0.12$	$10.2 \pm 3.1$
ViT + Llama	218.12	$0.84 \pm 0.11$	$8.1 \pm 2.9$
ViT + Mistral	218.12	$0.74 \pm 0.13$	$12.8 \pm 3.2$
ViT + Qwen	233.06	$0.82 \pm 0.13$	$9.7 \pm 3.1$
ViT + Yi	202.39	$0.86 \pm 0.12$	$7.9 \pm 3.3$

Table 3. Performance comparison of different ViT models combined with various LLMs for Task01.

while maintaining a manageable model size. In contrast, the ViT + Gemma model, despite having the highest number of parameters (264.25 million), does not provide the best performance, underscoring that an increased parameter count does not necessarily correlate with improved outcomes.

Among the LLMs evaluated, both Llama and Yi show notable improvements in segmentation metrics. The ViT + Llama model achieves a high Dice score of 0.84 and a low HD95 of 8.1, indicating effective performance and boundary precision. The results highlight that the Yi LLM outperforms other models in both accuracy and computational efficiency, making it a highly effective choice for enhanc-

ing medical image segmentation. Overall, the findings suggest that integrating advanced LLMs like Yi and Llama can significantly improve model performance while optimizing computational resources, making them preferable options over models with higher parameter counts but lower effectiveness.